Raman scattering investigation of RB_6 (R=Ca, La, Ce, Pr, Sm, Gd, Dy, and Yb)

Norio Ogita,* Shinji Nagai, Naoki Okamoto, and Masayuki Udagawa
Faculty of Integrated Arts and Sciences, Hiroshima University, Hiroshima 739-8521, Japan

Fumitoshi Iga and Masafumi Sera
Graduate School of Advanced Sciences of Matter, Hiroshima University, Hiroshima 739-8530, Japan

Jun Akimitsu
Department of Physics, Aoyama-Gakuin University, Tokyo 157-8521, Japan

Satoru Kunii
Department of Physics, Graduate School of Science, Tohoku University, Sendai 980-8578, Japan
(Received 26 August 2003; published 30 December 2003)

The excitation-energy, polarization, and temperature dependeces of Raman scattering spectra have been measured for the RB_6 crystals ($R=Ca^{2+}$, La^{3+}, Ce^{3+}, Pr^{3+}, $Sm^{2.6+}$, Gd^{3+}, Dy^{3+}, and Yb^{2+}). In the divalent crystals of CaB_6 and YbB_6, the E_g phonon shows doublet, while the line shape is a broad single peak for the trivalent case. In the trivalent crystals, two kinds of the extra peaks have been clearly observed at around 200 cm^{-1} and at around 1400 cm^{-1} in addition to the Raman-active phonons and crystal electric-field (CEF) excitations. The peak intensities at around 200 cm^{-1} show the anomalous decrease with decreasing temperature, and this temperature dependence correlates with that of the mean-square displacement of the R ion. Furthermore, their energies decrease with the increase of the cage space due to B_6. These peaks are originated from the second-order excitation of acoustic phonons. The broad peak at around 1400 cm^{-1} is assigned as the second-order excitation of the T_{2g} phonon. For the T_{2g} phonon, the energy difference and its line-shape change between the trivalent and divalent crystals suggests the existence of electron-phonon interaction. We have observed the CEF excitation in PrB_6 and have obtained the Lea, Leask, and Wolf parameters with $x=0.94$ and $W=9.2$ K.

DOI: 10.1103/PhysRevB.68.224305 PACS number(s): 63.20.−e, 78.30.−j

I. INTRODUCTION

Rare-earth hexaborides, RB_6, crystallize in a CsCl-type structure with $Pm3m$ symmetry, where a rare-earth ion occupies a Cs site and octahedral B_6 molecule locates on the Cl site.[1] These boron ochtahedra are linked together by very strong covalent bonds, which is the origin of the hardness of the crystals. The isostructural compounds of RB_6 exhibit interesting physical properties, such as superconductivity in YB_6,[2] dense Kondo behavior in CeB_6,[3] and an intermediate-valence state in SmB_6.[4] It is well known that trivalent rare-earth hexaborides are monovalent metals. Actually, LaB_6 is one of the most typical monovalent metals.[5] On the other hand, nonmagnetic divalent rare-earth hexaborides such as YbB_6 are known as typical narrow gap semiconductors.[6] The electronic conduction is well explained by the results of the band calculation.[7] A semiconductor SmB_6 is a special compound, where the Sm ion has both $4f^6$ and $4f^5$ configurations ($4f^6$:$4f^5 \simeq 3$:7).[8–10]

The investigation of the crystal electric-field (CEF) splitting of rare-earth ions is important. The energy splitting of the CEF for rare-earth hexaborides has been directly observed by inelastic neutron and Raman scatterings. The observed CEF energy splitting of CeB_6 is 530 K from the Γ_8 ground state to the Γ_7 excited state.[11] Based on the CEF knowledge, the recent investigation reveals a multiple-ordered phase in the H-T phase diagram.

In addition to CEF, the importance of lattice dynamics has been pointed out by Kunii *et al.*, who explained the anomaly of specific heat around 40 K of CeB_6 by the contribution of the flat branches of acoustic phonons.[12] The electric resistivity of LaB_6 is well explained by the electron scattering due to both optical and acoustic phonons.[13] Mandrus *et al.* pointed out that the local vibrational mode of the rare-earth ion contributes to not only specific heat but also resistivity.[14] Their proposed concept of ''oversized cage of borons'' is a key phrase in this paper. Observed and calculated phonon dispersion curves have been reported in Refs. 12, 15 and 16. Takegahara and Kasuya employed the volume-dependent and long-range force acting on rare-earth ions, in order to reproduce the phonon dispersion curves for LaB_6 and YbB_6.

To investigate both CEF excitations and lattice vibrations, Raman scattering is a useful tool. The Raman scattering spectra of CEF excitations for CeB_6 (Ref. 11) and NdB_6 (Ref. 17) have been reported by Zirngiebl and Pofahl. The Raman-active phonons in RB_6 are the vibrations of borons, which are the breathing and deforming modes of the octahedral B_6. The phonon Raman spectra were investigated by several groups.[18–25] They found the decrease of phonon energy with increasing lattice parameter by substitution of R ions, and also the valence dependence of the B_6 vibration.

Except for the CEF excitations and phonons, Zirngiebl *et al.* observed an anomalous ''one'' peak at around 200 cm^{-1}, of which energy decreases with the decrease of lattice parameter,[25] and they assigned this peak as the ''optical'' T_{1u} mode at the Γ point from the comparison with the

observed phonon-dispersion curves for only LaB_6. For the spectra in SmB_6, Mörke *et al.* assigned this peak as the defect-induced mode.[26] However, Lemmens *et al.*[23] and Nyhus *et al.*[27] assigned the peak as two-phonon scattering of the LA phonon at the Brillouin-zone boundary. Thus the origin of this anomalous low-energy peak is still controversial.

Our recent works of Raman scattering of RB_6 have suggested that the number of anomalous peaks at the low-energy region is not a single peak, but three. Furthermore, a new broad peak is observed at the higher energy region of the phonons.[28] For the phonons, we have also found that the line shape of the E_g phonon depends on the valence of the R ion.[29] Therefore recent development of the research leads us to re-study the lattice dynamics, the electronic state, and the relationship between them for RB_6. In this study, we have employed a different valent compound of RB_6 ($R=Ca^{2+}$, La^{3+}, Ce^{3+}, Pr^{3+}, $Sm^{2.6+}$, Gd^{3+}, Dy^{3+}, and Yb^{2+}), and the polarization, temperature, and excitation-energy dependence have been measured for each sample. In this paper, among several excitations observed in the Raman spectra, we mainly report the results of the peaks at about 200 cm^{-1}, which is the controversial mode described above. In this report, we name the peaks as extra modes.

The paper is organized as follows. Section II describes the detailed experimental procedure. We present the experimental results in Sec. III and discuss the origin of the observed mode and the electron-phonon interaction in Sec. IV.

II. EXPERIMENTAL

The samples of the present study were prepared by the following methods. Polycrystalline samples of CaB_6 were grown by a solid-state reaction of CaO and B powder. The powder mixtures were pressed into pellets and sintered at 1650 °C for 2.5 h in the reduction atmosphere. The sample characterization was done by a powder x-ray diffraction, and the obtained patterns have confirmed the single phase with the cubic hexaboride structure.

The single-crystalline samples YbB_6, SmB_6, and LaB_6 were grown by a floating-zone method using an image furnace with four xenon lamps, after a borothermal reaction $R_2O_3+15B \rightarrow 2RB_6+3BO\uparrow$ ($R=$Yb, La, and Sm) in vacuum by a radio frequency induction furnace.[30] The other single crystals of RB_6 ($R=$Pr, Ce, Gd, and Dy) were grown by a floating-zone method.[31]

Raman scattering spectra were measured by the following multichannel detection systems. An Ar ion laser operated at 488.0 or 514.5 nm and a dye laser operated at 570–633 nm were employed as an excitation light with the output power of 10 mW. Two different Raman scattering systems were employed: so-called macro- and micro-Raman systems. The scattered light was analyzed by a triple monochromator (JASCO model U-1800), and the analyzed light was detected by a liquid N_2 cooled charge-coupled device (CCD) detector (Princeton Instruments Inc. model LN/CCD-1100-PB).

The $Pm3m$ symmetry gives us the phonon numbers at Brilloiun-zone center; $\Gamma=A_{1g}+E_g+T_{1g}+T_{2g}+3T_{1u}+T_{2u}$. The T_{1u} representation includes one acoustic phonon. The Raman-active phonons are A_{1g}, E_g, and T_{2g}, which are the vibration of boron octahedra. Two T_{1u} modes are infrared active, and T_{1g} and T_{2u} are optically inactive. In this cubic symmetry, all Raman-active phonons appear in the $(x+y,x+y)$ polarization geometry. In the notation of (a,b), a and b denote the polarization directions of incident and scattered light, respectively. In this study, a and b correspond to the crystal axes of [100] and [010], respectively.

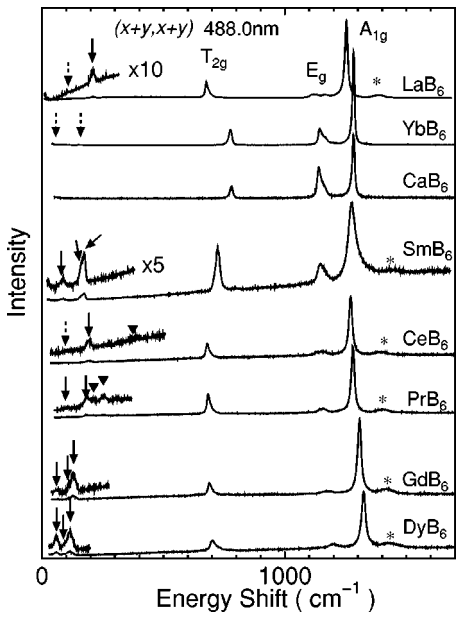

FIG. 1. Raman spectra of RB_6 ($R=$Ca, La, Ce, Pr, Sm, Gd, Dy, and Yb) at room temperature and at the 488.0-nm excitation. The spectra are depicted in the order of the decreasing lattice constants from top to bottom. The dotted and solid arrows denote extra modes discussed in this paper. The peaks by dotted arrows appear in the spectra excited by ~602-nm energy. Triangles are CEF excitations.

III. RESULTS

A. Overview of the Raman spectra of RB_6

Figure 1 shows the Raman spectra of RB_6 at room temperature. Each spectrum is depicted in the order of the decreasing lattice constants from top to bottom. Among them, $R=$Yb and Ca are divalent ions, Sm has the intermediate valence, and the others are trivalent. Three observed peaks at around 700, 1200, and 1300 cm^{-1} are the Raman-active phonons with the representations of T_{2g}, E_g, and A_g, respectively, and they completely satisfy the polarization selection rule in the cubic symmetry.

As shown in Fig. 1, the following spectral difference between divalent cation crystals and the others is found. An extra mode below 200 cm^{-1} and a broad peak at ~1400 cm^{-1}, denoted by arrows and asterisks, are commonly observed with a relatively strong intensity for trivalent and intermediate-valent crystals. However, for the divalent case, it is difficult to recognize of the existence of the extra peaks in this vertical scale owing to their too weak intensity. In addition, the line shape of the T_{2g} phonon for the trivalent R case is asymmetric but symmetric for divalent, and the E_g phonons is a broad single peak for the triva-

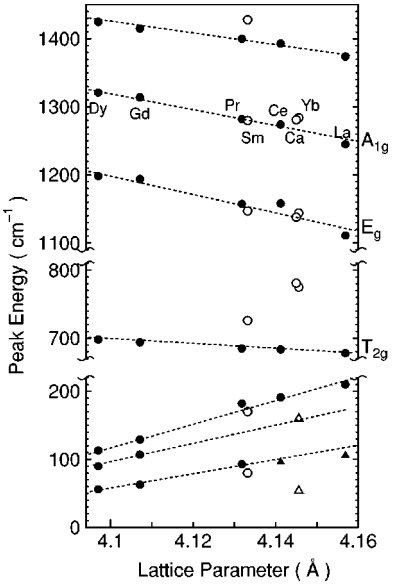

FIG. 2. Observed peak energy vs lattice parameter. The closed marks denote trivalent cations, and open ones are for divalent (Ca and Yb) and intermediate-valent (Sm) cations. The open and closed triangles denote the observed peaks at the lower energy excitation spectra. The dotted lines are a guide for the eye.

lent case but a doublet for divalent. The results clearly show that the phonon line shape strongly depends on the valence of *R* and also their electronic conductivity.

The lattice parameter dependence of the observed peak energy is shown in Fig. 2, where interesting results of the extra modes and the broad peak at the highest energy region are also included. The similar dependence for T_{2g}, E_g, A_g, and one of the extra modes around 200 cm^{-1} have been reported.[22,25] Among them, the dependence of the Raman-active phonons is normal, since their energies increase with decreasing the lattice parameter. However, all extra modes below 200 cm^{-1} have opposite correlation against the phonons. As shown in Fig. 2, the low-energy three lines suggest that the number of the extra modes is essentially 3. As shown in Fig. 1, three peak spectra of the extra modes become clear for the sample with the smaller lattice parameter, such as Dy and Gd cases, while the clear mode is one for La. In the divalent case at the 488.0-nm excitation, no extra mode is observed in spite of the middle lattice parameter between the La and Ce samples. This valence dependence concludes that the low-energy extra modes and the peaks at $\sim$1400 cm^{-1} clearly appear for the metallic or semiconductive samples.

B. Excitation energy dependence

The excitation energy dependencies of the representative spectra of Ce, Gd, Sm, and Yb are shown in Fig. 3. The intensity of each spectrum is normalized by that of A_g. The intensity of E_g and T_{2g} decreases with the decrease of the excitation energy, but that of the extra modes increases. In the CeB_6 spectra, the new peak appears at about 100 cm^{-1} at the 602.5-nm excitation, and the similar peak is obtained at 514.5-nm excitation for LaB_6. These new peaks are marked by the dotted arrows in Fig. 1 and their energies are also plotted by the closed triangles in Fig. 2. Although the extra modes have not been observed in YbB_6 at the 488.0-nm excitation as shown in Fig. 1, the broad small peaks at around 160 cm^{-1} appear at 602.5 nm. This is also marked by the dotted arrows in Fig. 1 and by the open triangles in Fig. 2. The energy at the lower energy excitation locates on the lines in Fig. 2. Thus these peaks can be regarded as one of extra modes. In SmB_6, similar results are obtained. However, there is no corresponding peaks for CaB_6 even at the red light excitation. Therefore the extra modes below 200 cm^{-1} appear for the samples with rare-earth ions.

Raman scattering occurs due to the second-order perturbation process in electronic system, so the scattering intensity depends on the excitation energy in consequence of the energy denominator of the Raman matrix elements. This re-

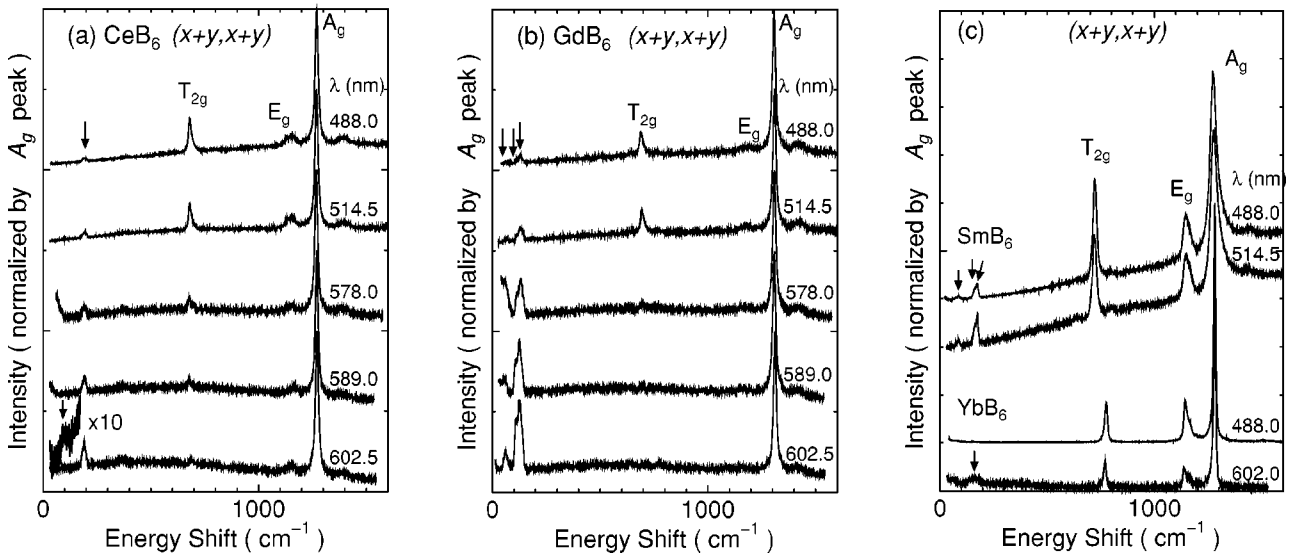

FIG. 3. Excitation energy dependence of Raman spectra at room temperature: (a) CeB_6, (b) GdB_6, and (c) mixed-valent SmB_6 and divalent YbB_6.

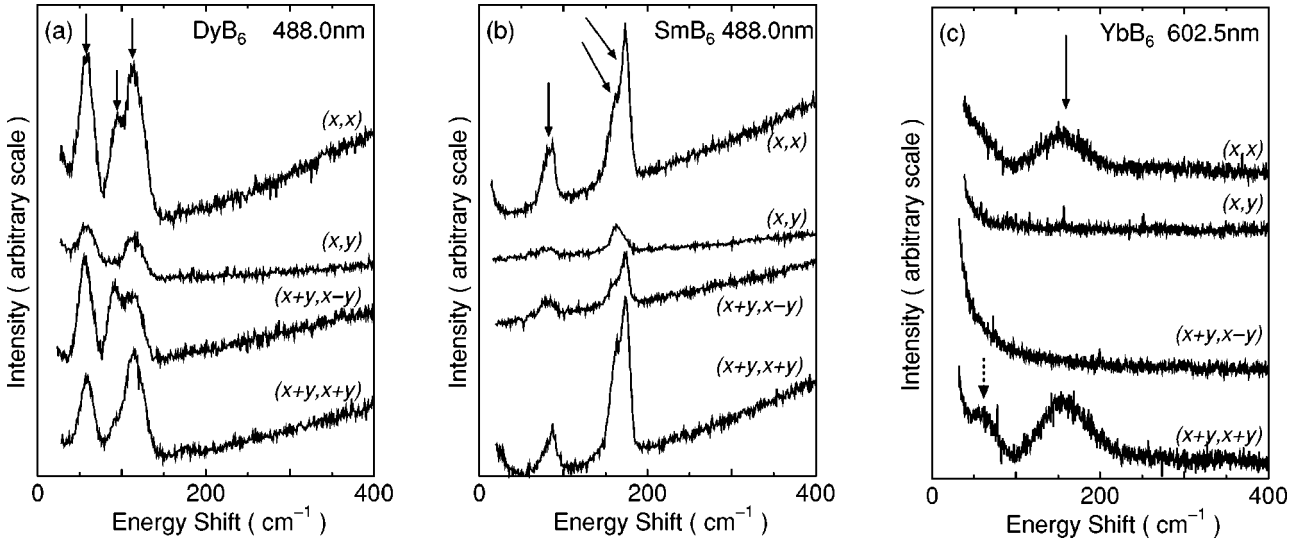

FIG. 4. Polarization dependence of the low-energy extra modes of (a) DyB_6, (b) SmB_6, and (c) YbB_6 in the energy region below 400 cm^{-1}. The spectra of DyB_6 and SmB_6 are the results measured at 488.0 nm and at 602.5 nm for YbB_6.

sult shows that the excitation process of the extra modes quite differs from that of the first-order phonons.

C. Polarization dependence

As mentioned above, the Raman-active phonons of RB_6, A_{1g}, E_g, and T_{2g}, completely satisfy the selection rules in the cubic symmetry, that is, A_{1g} phonon is observed in (i,i) spectra $(i=x,y,z)$, E_g in (i,i) and $(x+y,x-y)$ spectra, and T_{2g} in (x,y). However, the extra modes have a poor polarization dependence as shown in Fig. 4, where the representative polarization dependencies measured at room temperature are shown. In the figures, $(x+y,x+y)$ spectra are also depicted. As shown in Fig. 4, all extra modes are observed in all polarization geometries for DyB_6 and SmB_6 spectra. Thus these modes are not originated from the first-order Raman scattering process. Furthermore these cannot be assigned as a defect-induced mode because of the systematic observation.

For YbB_6, a similar resonance effect has been observed as the trivalent case. However, the polarization dependence is quite different from that of trivalent case, since the mode appears in only (i,i) spectra, that is, A_{1g}. In addition, the linewidth is much broader than that for the trivalent case.

D. Temperature dependence of the low-energy extra modes

The representative temperature dependence of Raman spectra of Dy, Sm, and Yb are depicted in Fig. 5. The remarkable feature is the decrease of the intensities with decreasing temperature without the line narrowing, as shown in Figs. 5(a) and 5(b). At 10 K, all modes in this energy region disappear for trivalent and intermediate crystals. For ordinary excitations, such as phonons and CEF excitations, the intensity increases and the linewidth becomes narrower with decreasing temperature owing to the suppression of thermal fluctuations.

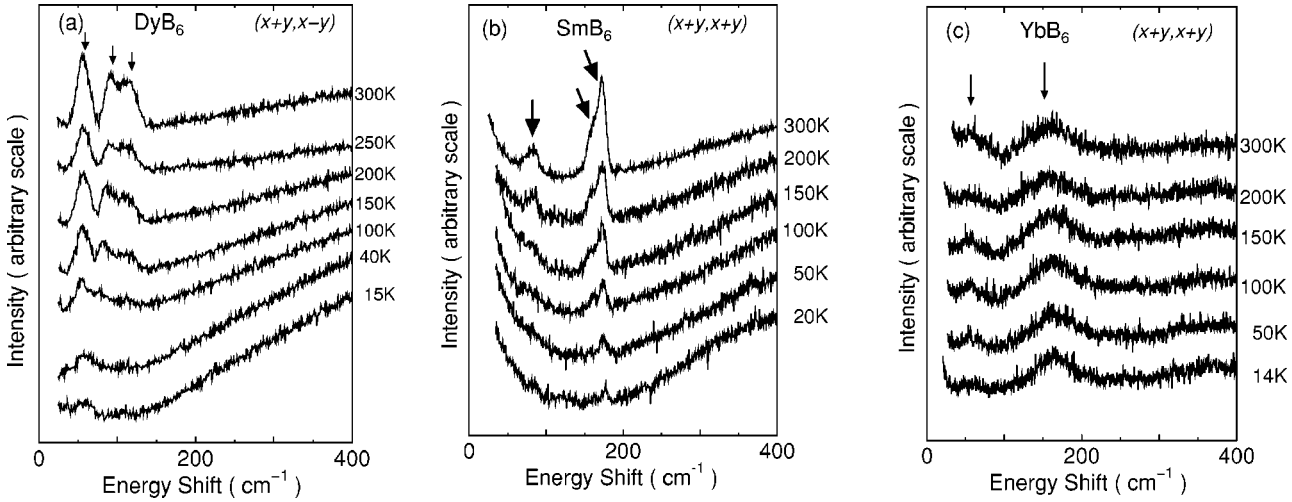

FIG. 5. Temperature dependence of Raman spectra for (a) DyB_6, (b) SmB_6, and (c) YbB_6 in the energy region below 400 cm^{-1}.

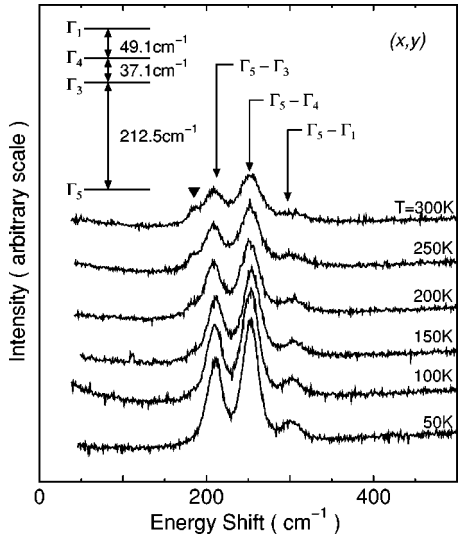

FIG. 6. Temperature dependence of Raman spectra for PrB_6. The inset denotes the crystal level scheme for PrB_6 determined by Raman scattering with Lea-Leask-Wolf (LLW) (Ref. 33) parameters $x=+0.94$ and $W=9.2$ K. The arrows indicate the CEF excitations between the levels with $x=0.94$ and $W=9.2$ K. The triangle indicates the extra mode.

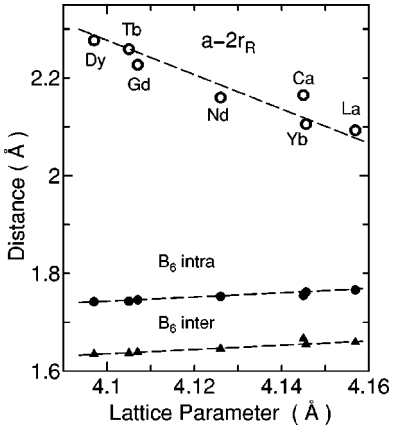

FIG. 7. Interatomic distance of inter and intra B_6 and cage space $a-2r_R$ vs lattice parameter. a is lattice parameter, and r_R is ionic radius of R (Ref. 36).

In SmB_6, a unique spectral feature is observed in the temperature dependence. As shown in Fig. 5(b), the low-energy continuum below 300 cm^{-1} is rapidly suppressed below 50 K. This is caused by the gap formation. For details we refer to the report by Nyhus *et al.*[27]

In the case of YbB_6 as shown in Fig. 5(c), the peak intensity is almost constant and does not vanish at low temperature. Therefore the extra modes in YbB_6 are quite different from the trivalent and intermediate-valent crystals.

We summarize here the results of the extra modes below 200 cm^{-1} for $R^{3+}B_6$ and SmB_6:

- the peaks are clearly observed in trivalent $R^{3+}B_6$ and SmB_6
- with increasing the lattice parameter, the energy systematically increases
- the peak width is broad compared with phonon's
- poor polarization dependence
- the intensity decreases to almost zero with decreasing temperature
- the excitation energy dependence differs from the phonons
- does not belong to the first-order Raman scattering process.

E. CEF excitation

The detailed CEF study has been performed by Zirngiebl and Pofahl for CeB_6 (Ref. 11) and NdB_6 (Ref. 17) by Raman scattering. The similar results are obtained in our work for CeB_6. Here we present the CEF excitation spectra of PrB_6, because there is no report of the CEF excitations of PrB_6 measured by Raman scattering. In neutron inelastic scattering, CEF of PrB_6 has been studied by Loewenhaupt and Prager.[32] They determined the CEF levels in the framework of the Lea-Leask-Wolf (LLW) scheme,[33] and obtained the LLW parameters of $x=+0.95$ and $W=9.5$ K.

The temperature dependence of (x,y) Raman spectra for PrB_6 is shown in Fig. 6, where three peaks at around 210, 250, and 300 cm^{-1} are the CEF excitations. Their intensity of CEF excitation increases with decreasing temperature.

The multiplet ground state of Pr^{3+} is split in a cubic crystal field into two triplets Γ_5 and Γ_4, a nonmagnetic doublet Γ_3, and a singlet Γ_1. Taking into account the observed energies of the peaks, we have estimated the CEF levels of Pr^{+3} in cubic field in the LLW scheme by the energy fitting. The inset in Fig. 6 denotes the determined CEF levels with the LLW parameters of $x=+0.94$ and $W=9.2$ K, and the corresponding transitions are marked by arrows. Since the irreducible representations for the transitions from Γ_5 to Γ_3, Γ_4, and Γ_1 include $\Gamma_4(T_{2g})$, the observed three peaks in the (x,y) spectra satisfy this polarization selection rule. We note that the obtained LLW parameters are consistent with those by neutron scattering.[32]

However, we should note that the relative intensity of the excitations $\Gamma_5 \rightarrow \Gamma_3$ and $\Gamma_5 \rightarrow \Gamma_4$ cannot be explained by the LLW theory. This is the remaining problem and it might be related to the Raman scattering process.

IV. DISCUSSION

The first discussion is the origin of the extra modes below 200 cm^{-1}. RB_6 is regarded as one of the clathrate compounds with the cage constructed by borons. The crystal structure is stabilized by strong B-B interactions of intra and inter octahedral B_6. On the other hand, the R ion weakly interacts with the surrounding 24 borons. Because of this weak interaction between R and octahedral B_6, the observed CEF excitation is explained by a point-charge model. In this structure, the characteristic atomic distances are inter B_6-B_6, intra B_6, and cation-boron distance. Each bond length is plotted as a function of lattice parameter in Fig. 7, using the results in Refs. 34 and 35. With increasing lattice parameter, the inter- and intra-atomic distances of B_6 slightly increase. Thus the lattice parameter dependence of the phonon energy

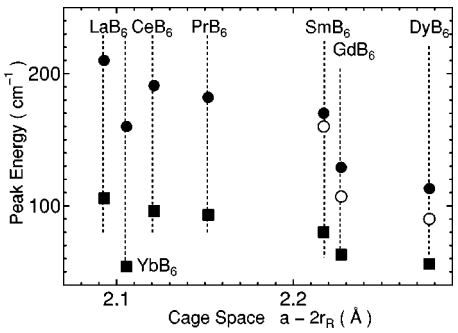

FIG. 8. The energy of the extra modes vs cage space $a-2r_{\mathrm{R}}$.

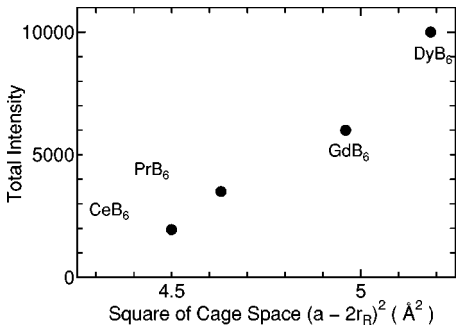

FIG. 9. Integrated intensity of the extra modes vs square of the cage space $(a-2r_{\mathrm{R}})^2$.

is well understood by this change as shown in Fig. 2. However, the $a-2r_{\mathrm{R}}$ decreases with increasing lattice parameter, where a and r_{R} are the lattice parameter and ionic radius of R, respectively.[36] $a-2r_{\mathrm{R}}$ can be regarded as the movable space of the R ion in the "cage space." The relationship between the energy of the extra modes and the cage space $a-2r_{\mathrm{R}}$ is plotted in Fig. 8. The dependence suggests that the extra modes relate to the movement of R ions in harmonic potential, which becomes shallow for the crystals with the shorter lattice parameter. This is the origin of the anomalous lattice parameter dependence of the extra modes below 200 cm^{-1}.

In the classical discussion about the Raman scattering process, the scattering intensity is proportional to square of the amplitude of atomic displacement. Therefore the amplitude of the R vibration increases with increasing cage space, because the larger cage space makes shallower effective potential at the position of R. Figure 9 shows the integrated peak intensity as a function of the square $a-2r_{\mathrm{R}}$. The integrated intensity is proportional to square of the effective cage space. This shows that the R ion has a large displacement for the crystals with the large cage space. Chernyshov *et al.*[37] determined the mean-square displacement (MSD) of the R ion for light rare-earth crystals with La, Ce, Pr, Nd, and Sm by x-ray diffraction. According to their result, the MSD of R is larger for the larger cage space of $a-2r_{\mathrm{R}}$. Therefore this discussion concludes that the origin of the extra modes is related to the movement of R in the B_6 cage.

In Ref. 37, the temperature dependence of the mean-square displacement (MSD) of the Sm ion has been also reported. The MSD of the Sm ion decreases with decreasing temperature. Figure 10(a) shows the intensity of the extra modes vs the MSD for SmB_6. The proportionality in Fig. 10(a) shows that the origin of the extra modes is related to the thermally activated movement of Sm. As mentioned in the previous section, the extra modes of SmB_6 (intermediate valence) has the same properties with that of the trivalent ones. Figures 10(b) and (c) present the relationship between the peak intensity of GdB_6 and DyB_6 vs the MSD of Sm, assuming a similar temperature dependence of the MSD for GdB_6 and DyB_6.

So far, we have mentioned that the extra modes are originated from the vibration of the R ion, judging from the results of the rare-earth and temperature dependencies. Before the present work, one of the extra modes was assigned as the optical T_{1u} mode at the Brilloiun-zone center. From the fac-

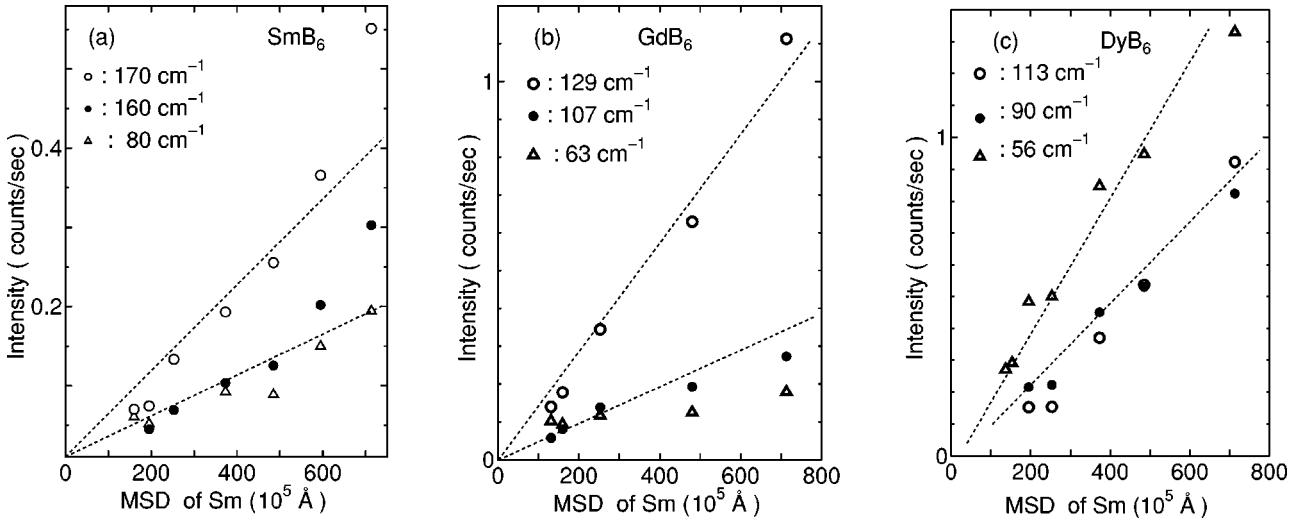

FIG. 10. Peak intensities vs MSD (a) SmB_6, (b) GdB_6, and (c) DyB_6. The employed MSD is the results for SmB_6 measured by Chernyshov *et al.* (Ref. 37).

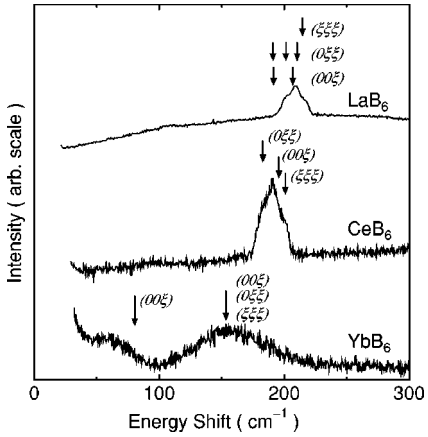

FIG. 11. Energy comparison with twice the energy of the acoustic phonon at Brillouin-zone boundary in all directions for LaB_6, CeB_6, and YbB_6. The spectra for LaB_6 are obtained by 514.5-nm excitation, and for CeB_6 and YbB_6 by 602.5-nm excitation. The arrows for LaB_6 and CeB_6 denote twice the energy of the observed phonon (Refs. 12 and 15), and for YbB_6 the calculated one (Ref. 16).

tor group analysis, there are two optical T_{1u} modes except for the acoustic mode. In our previous infrared absorption measurement,[38] another T_{1u} mode is observed at around 900 cm^{-1} for CeB_6 and YbB_6. If the extra modes have the symmetry of T_{1u}, the mode at around 900 cm^{-1} should be observed in the Raman spectra. However, there are no peaks at the corresponding energy region.

Poor polarization dependence of the extra modes strongly suggests the possibility of the second-order Raman process. The selection rule of the second-order excitation for T_{1u} is derived from the direct product $T_{1u} \otimes T_{1u}$. This direct product is decomposed to A_{1g}, E_g, T_{1g}, and T_{2g}. Among these, A_{1g}, E_g, and T_{2g} are Raman active. Therefore the second-order T_{1u} excitation should be detected in all polarization geometries and this polarization property agrees with the experimental results as shown Figs. 4(a) and 4(b). Furthermore, in order to check this process, we compare the energy of the extra modes with that of the observed[12,15] and calculated[12,16] phonon-dispersion curve. The branches of LA and TA have the wide flat region in the Brillouin zone along (00ξ), $(0\xi\xi)$, and $(\xi\xi\xi)$. Their energy at the zone boundary is 90–100 cm^{-1} for CeB_6, 43–77 cm^{-1} for YbB_6, and 95–107 cm^{-1} for LaB_6. The flat dispersion gives rise to the large density of states, and twice their energies agree with the energy of the extra modes as shown in Fig. 11, where the arrows denote twice the energy of LA and TA phonons at the Brillouin-zone boundary for CeB_6, LaB_6, and YbB_6. Except for the lowest mode of La and Ce, this good agreement concludes that the extra modes originate from the second-order Raman scattering of acoustic branches at the Brillouin-zone boundary. To visualize the vibration, the atomic displacements for each irreducible representation are shown in Fig. 12. The Raman active modes, A_{1g}, E_g, and T_{2g}, are breathing and deformation vibrations of octahedral B_6. Among three T_{1u} modes, the T_{1u}-1 mode corresponds to the acoustic phonon, which includes the R ion displacement.

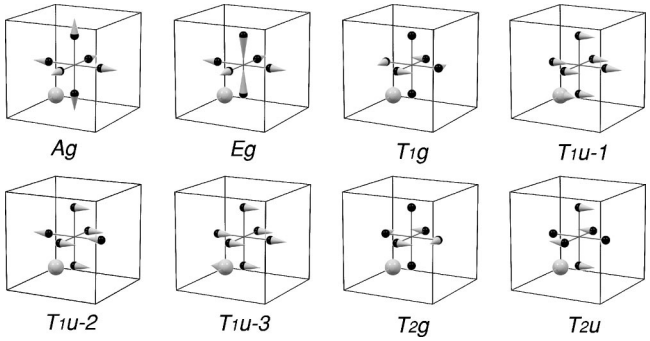

FIG. 12. Atomic displacement of the phonon mode.

From the above discussion, it is experimentally clarified that the extra modes below 200 cm^{-1} originate from the second-order Raman process for the thermally excited T_{1u} mode at the Brillouin-zone boundary. However, it remains why the anomalous intensity decrease at low temperature occurs only for the conductive crystals, since the intensity decrease has not been observed for the divalent crystals. Thus the conduction electron is important. This problem is an open question at this stage, but we can make the following comments qualitatively. T_{1u} is a polar vibration, which induces electric dipole moment due to displacements. Probably free electron at the zone boundary easily couples with this vibration, and this coupling would increase the electronic polarizability of the vibration. In fact, the intensity of the conductive samples is stronger than that of YbB_6. Unfortunately, we do not know the precise electron density of states at the zone boundary at the corresponding low-energy region. If this speculation is correct, this is a different type of interaction between the R ions in the hexaboride crystals assisted by conduction electrons. Therefore we need the theoretical support to clarify this problem.

As other related topics with the anomalous low-energy extra modes, we can point out the temperature dependence of the intensity of the single excitation of the acoustic phonon at the Brillouon-zone boundary. Unfortunately, this is out of range of Raman scattering. The inelastic neutron scattering is necessary to clarify this.

Once we reported that the extra modes relate to a ''rattling mode'' of the R ion.[28] The rattling mode of the R ions is understood as the independent vibration in each cage without the R-R interactions, that is, Einstein oscillation. The existence of the Einstein mode was reported by Mandrus.[14] The thermally activated vibration of R in the B cage is decomposed to the incoherent and coherent motion. The former corresponds to the rattling mode and the latter to the acoustic branch. The present detailed study shows that the extra modes cannot be regarded as the independent mode, but the coherent mode with long-range interaction between R ions. The importance of the nearest- and the next-nearest-neighbor interactions between the R ions has been already predicted by the calculation of phonon-dispersion curves of RB_6.[16]

Next we discuss the T_{2g} mode. As shown in Fig. 2, all peak energies of A_{1g} and E_g lie on the single line shown by the dotted line. However, for T_{2g}, the energy difference is $\sim$100 cm^{-1} between the trivalent and divalent crystals. The

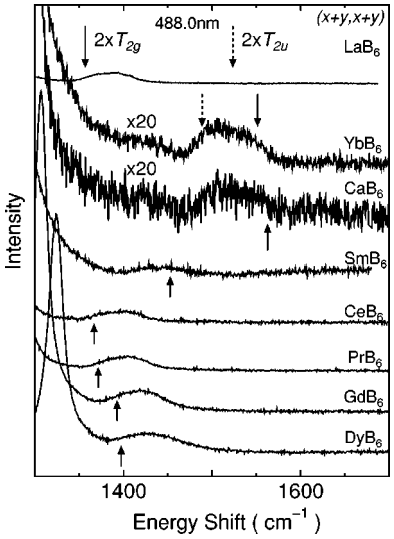

FIG. 13. Raman spectra of RB_6 in the energy region 1300–1700 cm^{-1}.

essential difference between them is the existence of the conduction electron. Thus for the trivalent case, the electron-phonon interaction can be expected. In fact, the line shape of the divalent crystal is symmetric, but asymmetric for the trivalent one. In SmB_6 with the lower concentration of conduction electron than that of the trivalent one, the line-shape asymmetry is weak. This qualitative discussion suggests to us the existence of the interference effect between the sharp phonon and a broad electronic response. However, for the quantitative discussion of the interference effect, the present results are not enough, such as the precise measurement of background intensity and detailed laser wavelength dependence. Here we only point out the possibility of the interference model. If there is the electron-phonon coupling, the energy of the coupled phonon might be suppressed by this interaction like the E_{2g} mode in MgB_2.[39] Here, we regard the energy of the divalent crystals as the uncoupled phonon energy, because their carrier density is very low. To discuss further using the present results, the lattice dynamical calculations based on the first principle is necessary, in order to determine the electron-phonon interaction coefficient directly from the energy change for T_{2g}.

We note here about the broad peak observed at around 1400 cm^{-1} for the trivalent crystals. Its symmetry is A_{1g} and E_g. This peak cannot be assigned as the phonons due to the first-order Raman process, since there is no phonon in the corresponding energy region, according to the phonon-dispersion calculation.[16] We can point out several possible mechanisms like electronic excitation, satellite peak of the first-order phonon, and second-order process. Among them, the second-order process is the most plausible for the following reasons. The Raman spectra in the energy region between $\sim$1300 and 1700 cm^{-1} is shown in Fig. 13.

We discuss the divalent case. For the divalent crystal, the vertical scale of the figure is enlarged by 20 times and its relative intensity to that of T_{2g} is almost 1% in the $(x+y,x+y)$ geometry. The arrows denote twice of the energy of T_{2g} and dashed line that of T_{2u}. Twice energies of the other branches are out of the energy region shown in Fig. 13. The energy coincidence is very good for the divalent ones. According to the phonon-dispersion curve of LaB_6 and YbB_6,[16] T_{2g} and T_{2u} have the flat dispersion from the Γ to X point in the Brillouin zone, which increases the density of states of the phonon. Then, the relative intensity and the good energy coincidence strongly suggest that the peak at 1400 cm^{-1} is explained by the second-order process for the divalent case.

For trivalent case, twice the energy of T_{2g} is slightly lower than the peak energy, however, the peak energy systematically follows twice the energy of T_{2g}. In LaB_6, the peak energy is far from twice the energy of T_{2u} and that of T_{2g} is very close to the peak energy. For SmB_6 the energy coincidence is very good. As another experimental fact of the relationship between the broad peak and T_{2g}, we point out the laser wavelength dependence as shown in Fig. 3, where the intensity of both spectra simultaneously decreases with increasing wavelength. Thus it can be concluded that the peak observed in the trivalent case originates from the second-order process of T_{2g}. We emphasize that the intensity of the peak is the same order of that of T_{2g} for the trivalent crystals. There is the problem of why this second-order peak has the strong intensity. To clarify this phenomena, the electron-phonon coupling of T_{2g} is important as described above. The depicted twice energy of T_{2g} for the trivalent crystals is the coupled energy, not the uncoupled energy, of which twice energy becomes 1600 cm^{-1}. Furthermore, the relative intensity to that of T_{2g} for SmB_6 is slightly weaker than that of the trivalent crystals, as shown in Fig. 1. Thus the observed peak energy corresponds to twice the coupled energy. At this stage, we cannot proceed the discussion further, since the density of states of the conduction electron is unclear, however, we believe that the present experimental results are important to clarify the electron-phonon interaction in RB_6 crystals. We note that the polarization dependence described above does not violate that for the second order of T_{2g}.

As the conclusion, we summarize the obtained main results. Two interesting modes at $\sim$200 and 1400 cm^{-1} are clearly observed for the trivalent crystals. The extra modes at around 200 cm^{-1} are assigned as the second-order excitations of the acoustic branch and their anomalous properties are related to the R ion movement in the cage constructed by B_6. On the other hand, the broad peak at around 1400 cm^{-1} is assigned as the second-order excitation of the T_{2g} phonon. For the T_{2g} phonon, the energy difference and its line-shape change between the trivant and divalent crystals suggest the existence of electron-phonon interaction. We have observed the CEF excitation in PrB_6 and obtained the LLW parameters with $x=0.94$ and $W=9.2$ K. However, the following problems remain for future work. The first is the intensity decrease at low temperature of the extra modes. The microscopic reason for why this decrease occurs for $R^{3+}B_6$ and SmB_6 is not clear. The second is the precise determination of the electron-phonon coupling in RB_6. The last is the relative intensity of CEF in PrB_6. To clarify these problems, theoretical support is necessary.

ACKNOWLEDGMENTS

This work was supported in part by a Grant-in-Aid for COE Research (Grant No. 13CE2002) of the Ministry of Education, Culture, Sports, Science and Technology of Japan. The low-temperature experiments were supported by the Natural Science Center for Basic Research and Development of Hiroshima University.

*Electronic address: nogita@hiroshima-u.ac.jp

[1] H. Hacher, Jr. and M.S. Lin, Solid State Commun. **6**, 37 (1968).
[2] S. Kunii, T. Kasuya, K. Kadowaki, M. Date, and S.B. Woods, Solid State Commun. **52**, 659 (1984).
[3] T. Komatsubara, N. Sato, S. Kunii, I. Oguro, Y. Furukawa, Y. Onuki, and T. Kasuya, J. Magn. Magn. Mater. **31-34**, 368 (1983).
[4] T. Kasuya, M. Kasaya, K. Takegahara, T. Fujita, T. Gotto, A. Tamaki, M. Takigawa, and H. Yasuoka, J. Magn. Magn. Mater. **31-34**, 447 (1983).
[5] Y. Ishizawa, T. Tanaka, E. Bannai, and S. Kawai, J. Phys. Soc. Jpn. **42**, 112 (1977).
[6] J.M. Tarascon, J. Etourneau, P. Dordor, P. Hagenmuller, M. Kasaya, and J.M.D. Coey, J. Appl. Phys. **51**, 574 (1980).
[7] A. Hasegawa and A. Yanase, J. Phys. F: Met. Phys. **7**, 1245 (1977).
[8] E.E. Vainshtein, S.M. Blokhin, and Yu.B. Paderno, Sov. Phys. Solid State **6**, 2318 (1965).
[9] A. Menth, E. Buehler, and T.H. Geballe, Phys. Rev. Lett. **22**, 295 (1969).
[10] R.L. Cohen, M. Eibschiitz, and K.W. West, Phys. Rev. Lett. **24**, 383 (1970).
[11] E. Zirngiebl, B. Hillebrands, S. Blumenrüder, G. Güntherodt, M. Loewenhaupt, J.M. Carpenter, K. Winzer, and Z. Fisk, Phys. Rev. B **30**, 4052 (1984).
[12] S. Kunii, J.M. Effantin, and J. Rossat-Mingnod, J. Phys. Soc. Jpn. **66**, 1029 (1997).
[13] T. Tanaka, T. Akahara, E. Bannai, S. Kawai, N. Tsuda, and Y. Ishizawa, J. Phys. C **9**, 1235 (1976).
[14] D. Mandrus, B.C. Sales, and R. Jin, Phys. Rev. B **64**, 012302 (2001).
[15] H.G. Smith, G. Dolling, S. Kunii, M. Kasaya, B. Liu, K. Takegahara, T. Kasuya, and T. Gotto, Solid State Commun. **53**, 15 (1985).
[16] K. Takegahara and T. Kasuya, Solid State Commun. **53**, 21 (1985).
[17] G. Pofahl, E. Zirngiebl, S. Blumenröder, H. Brenten, G. Güntherodt, and K. Winzer, Z. Phys. B: Condens. Matter **66**, 339 (1986).
[18] K. Kojima, K. Ohbayashi, T. Hihara, S. Kunii, T. Komatsubara, and T. Kasuya, Phys. Lett. **72A**, 51 (1979).
[19] Z. Yahia, S. Turrell, G. Turell, and J.P. Mercurio, J. Mol. Struct. **224**, 303 (1990).
[20] G. Güntherodt, R. Merlin, A. Frey, and M. Cardona, Solid State Commun. **27**, 551 (1978).
[21] H. Scholz, W. Bauhofer, and K. Ploog, Solid State Commun. **18**, 1539 (1976).
[22] M. Ishii, M. Aono, S. Muranaka, and S. Kawai, Solid State Commun. **20**, 437 (1976).
[23] P. Lemmens, A. Hoffman, A.S. Mishchenko, M.Yu. Talantov, and G. Güntherodt, Physica B **206 & 207**, 371 (1995).
[24] M. Ishii, T. Tanaka, E. Bannai, and S. Kawai, J. Phys. Soc. Jpn. **41**, 1075 (1976).
[25] E. Zirngiebl, S. Blumenröder, R. Mock, and G. Güntherodt, J. Magn. Mag. Mater. **54-57**, 539 (1986).
[26] I. Mörke, V. Dvorak, and P. Wachter, Solid State Commun. **40**, 331 (1981).
[27] P. Nyhus, S.L. Cooper, Z. Fisk, and J. Sarrao, Phys. Rev. B **55**, 12 488 (1997).
[28] N. Ogita, S. Nagai, N. Okamoto, M. Udagawa, F. Iga, M. Sera, J. Akimitsu, and S. Kunii, Physica B **329-333**, 661 (2003); **328**, 131 (2003).
[29] N. Ogita, S. Nagai, N. Okamoto, F. Iga, S. Kunii, T. Akamtsu, J. Akimitsu, and M. Udagawa, J. Solid State Chem. (to be published).
[30] F. Iga, N. Shimizu, and T. Takabatake, J. Magn. Magn. Mater. **177-181**, 337 (1998).
[31] S. Kunii, J. Phys. Soc. Jpn. **57**, 361 (1988).
[32] M. Loewenhaupt and M. Prager, Z. Phys. B: Condens. Matter **62**, 195 (1986).
[33] K.R. Lea, M.J.M. Leask, and W.P. Wolf, J. Phys. Chem. Solids **23**, 1381 (1962).
[34] M.M. Korsukova, Jpn. J. Appl. Phys., Part 1 **10**, 15 (1994).
[35] M.K. Blomberg, M.J. Merisalo, M.M. Korsukova, and V.N. Gurin, J. Alloys Compd. **217**, 123 (1995).
[36] R.D. Shanon, Acta Crystallogr., Sect. A: Cryst. Phys., Diffr., Theor. Gen. Crystallogr. **32**, 751 (1976).
[37] D.Yu. Chernyshov, M.B. Smirnov, A.V. Menschikova, A.P. Mirgorodsky, and V.A. Trounov, Physica B **234-236**, 146 (1997).
[38] M. Udagawa, S. Nagai, N. Ogita, F. Iga, R. Kaji, R. Sumida, J. Akimitsu, S. Kunii, R. Suzuki, H. Onodera, and Y. Yamaguchi, J. Phys. Soc. Jpn. **Suppl. 71**, 314 (2002).
[39] K.-P. Bohnen, R. Heid, and B. Renker, Phys. Rev. Lett. **86**, 5771 (2001).